

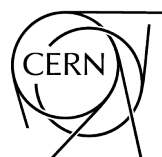
CERN Yellow Reports: Monographs
Volume 2/2017

CERN–2017–002–M

Handbook of LHC Higgs cross sections: 4. Deciphering the nature of the Higgs sector

Report of the LHC Higgs Cross Section Working Group

Editors: D. de Florian
C. Grojean
F. Maltoni
C. Mariotti
A. Nikitenko
M. Pieri
P. Savard
M. Schumacher
R. Tanaka



CERN Yellow Reports: Monographs

Published by CERN, CH-1211 Geneva 23, Switzerland

ISBN 978-92-9083-442-7 (paperback)

ISBN 978-92-9083-443-4 (PDF)

Print ISSN 2519-8068

Online ISSN 2519-8076

DOI <https://doi.org/10.23731/CYRM-2017-002>

Accepted for publication by the CERN Report Editorial Board (CREB) on 6 April 2017

Available online at <http://publishing.cern.ch/> and <http://cds.cern.ch/>

Copyright © CERN, 2017

 Creative Commons Attribution 4.0

Knowledge transfer is an integral part of CERN's mission.

CERN publishes this report Open Access under the Creative Commons Attribution 4.0 license (<http://creativecommons.org/licenses/by/4.0/>) in order to permit its wide dissemination and use. The submission of a contribution to a CERN Yellow Report series shall be deemed to constitute the contributor's agreement to this copyright and license statement. Contributors are requested to obtain any clearances that may be necessary for this purpose.

This volume is indexed in: CERN Document Server (CDS), INSPIRE.

This volume should be cited as:

LHC Higgs Cross Section Working Group, D. de Florian, C. Grojean, F. Maltoni, C. Mariotti, A. Nikitenko, M. Pieri, P. Savard, M. Schumacher, R. Tanaka (Eds.), Handbook of LHC Higgs Cross Sections: 4. Deciphering the nature of the Higgs sector, CERN Yellow Reports: Monographs, Vol. 2/2017, CERN-2017-002-M (CERN, Geneva, 2017), <https://doi.org/10.23731/CYRM-2017-002>

Abstract

This Report summarizes the results of the activities of the LHC Higgs Cross Section Working Group in the period 2014–2016. The main goal of the working group was to present the state-of-the-art of Higgs physics at the LHC, integrating all new results that have appeared in the last few years. The first part compiles the most up-to-date predictions of Higgs boson production cross sections and decay branching ratios, parton distribution functions, and off-shell Higgs boson production and interference effects. The second part discusses the recent progress in Higgs effective field theory predictions, followed by the third part on pseudo-observables, simplified template cross section and fiducial cross section measurements, which give the baseline framework for Higgs boson property measurements. The fourth part deals with the beyond the Standard Model predictions of various benchmark scenarios of Minimal Supersymmetric Standard Model, extended scalar sector, Next-to-Minimal Supersymmetric Standard Model and exotic Higgs boson decays. This report follows three previous working-group reports: *Handbook of LHC Higgs Cross Sections: 1. Inclusive Observables* (CERN-2011-002), *Handbook of LHC Higgs Cross Sections: 2. Differential Distributions* (CERN-2012-002), and *Handbook of LHC Higgs Cross Sections: 3. Higgs properties* (CERN-2013-004). The current report serves as the baseline reference for Higgs physics in LHC Run 2 and beyond.

We, the authors, would like to dedicate this Report to the memory of

Guido Altarelli (1941 - 2015)

Thomas Kibble (1932 - 2016)

and

Yoichiro Nambu (1921 - 2015)

Conveners

WG1: Higgs XS& BR: B. Mellado, P. Musella, M. Grazzini, R. Harlander

- *BR:* A. Denner, S. Heinemeyer, A. Mück, I. Puljak, D. Rebuzzi
- *ggF:* S. Forte, D. Gilberg, C. Hays, A. Lazopoulos, A. Massironi, G. Petrucciani, G. Zanderighi
- *VBF and WH/ZH:* S. Dittmaier, P. Govoni, B. Jäger, J. Nielsen, L. Perrozzi, E. Pianori, A. Rizzi, F. Tramontano
- *ttH/tH:* S. Guindon, C. Neu, S. Pozzorini, L. Reina

WG2: Higgs properties: M. Chen, M. Dührssen, A. David, A. Falkowski, C. Hays, G. Isidori

WG3: BSM Higgs: N. Rompotis, M. Pelliccioni, I. Low, M. Mühlleitner, R. Wolf

- *MSSM neutral:* R. Lane, S. Liebler, A. McCarn, P. Slavich, M. Spira, D. Winterbottom
- *MSSM charged:* M. Flechl, S. Sekula, M. Ubiali, M. Zaro
- *NMSSM:* U. Ellwanger, M. Mühlleitner, F. Staub, D. Strom, R. Yohay
- *Neutral extended scalars:* R. Gerosa, H. Logan, O. Stål, R. Santos, S. Su, X. Sun
- *Exotic decay:* S. Bressler, S. Gori, A. Mohammadi, J. Shelton

Cross-group task forces:

- *bbH/bH:* M. Beckingham, A. Nikitenko, M. Spira, M. Wiesemann
- *HH:* S. Dawson, C. Englert, M. Gouzevitch, R. Salerno, M. Slawinska
- *Fiducial cross-sections:* F.U. Bernlochner, S. Kraml, P. Milenovic, P. Monni
- *Offshell Higgs:* F. Caola, Y. Gao, N. Kauer, L. Soffi, J. Wang
- *MCnet:* S. Plätzer
- *PDF:* S. Forte, J. Huston, R. Thorne

Authors

D. de Florian¹, C. Grojean^{2,3,4,5}, F. Maltoni⁶, C. Mariotti⁷, A. Nikitenko⁸, M. Pieri⁹, P. Savard^{10,11}, M. Schumacher¹², R. Tanaka¹³ (Eds.), R. Aggleton^{14,15,16}, M. Ahmad¹⁷, B. Allanach¹⁸, C. Anastasiou¹⁹, W. Astill²⁰, S. Badger²¹, M. Badziak^{22,23,24}, J. Baglio²⁵, E. Bagnaschi², A. Ballestrero⁷, A. Banfi²⁶, D. Barducci²⁷, M. Beckingham²⁸, C. Becot^{13,29}, G. Bélanger²⁷, J. Bellm³⁰, N. Belyaev³¹, F.U. Bernlochner³², C. Beskidt³³, A. Biekötter³⁴, F. Bishara²⁰, W. Bizon²⁰, N.E. Bomark³⁵, M. Bonvini²⁰, S. Borowka³⁶, V. Bortolotto^{37,38,39}, S. Boselli⁴⁰, F.J. Botella⁴¹, R. Boughezal⁴², G.C. Branco⁴³, J. Brehmer⁴⁴, L. Brenner⁴⁵, S. Bressler⁴⁶, I. Brivio⁴⁷, A. Broggio⁴⁸, H. Brun⁴⁹, G. Buchalla⁵⁰, C.D. Burgard¹², A. Calandri⁵¹, L. Caminada³⁶, R. Caminal Armadans⁵², F. Campanario^{53,54}, J. Campbell⁵⁵, F. Caola^{56,30}, C.M. Carloni Calame⁵⁷, S. Carrazza⁵⁶, A. Carvalho⁵⁸, M. Casolino⁵, O. Cata⁵⁰, A. Celis⁵⁰, F. Cerutti²⁴, N. Chanon⁵⁹, M. Chen¹⁷, X. Chen⁶⁰, B. Chokoufé Nejad², N. Christensen⁶¹, M. Ciuchini⁶², R. Contino^{63,56}, T. Corbett⁶⁴, R. Costa^{56,65}, D. Curtin⁶⁶, M. Dall'Osso⁵⁸, A. David⁵⁶, S. Dawson⁶⁷, J. de Blas⁶⁸, W. de Boer³³, P. de Castro Manzano⁵⁸, C. Degrande³⁰, R.L. Delgado⁶⁹, F. Demartin⁶, A. Denner⁷⁰, B. Di Micco⁷¹, R. Di Nardo⁵⁶, S. Dittmaier¹², A. Dobado⁶⁹, T. Dorigo⁵⁸, F.A. Dreyer^{72,73,56}, M. Dührssen⁵⁶, C. Duhr^{56,6}, F. Dulat⁷⁴, K. Ecker⁷⁵, K. Ellis³⁰, U. Ellwanger⁷⁶, C. Englert⁷⁷, D. Espriu⁷⁸, A. Falkowski⁷⁶, L. Fayard¹³, R. Feger⁷⁰, G. Ferrera⁷⁹, A. Ferroglio^{80,81}, N. Fidanza^{82,1}, T. Figy⁸³, M. Flechl⁸⁴, D. Fontes⁴³, S. Forte⁸⁵, P. Francavilla^{86,87}, E. Franco⁶⁸, R. Frederix⁴⁸, A. Freitas⁸⁸, FF. Freitas²⁶, F. Frensch³³, S. Frixione⁸⁹, B. Fuks^{72,73}, E. Furlan¹⁹, S. Gadatsch⁵⁶, J. Gao⁴², Y. Gao⁹⁰, M.V. Garzelli⁹¹, T. Gehrmann³⁶, R. Gerosa⁹, M. Ghezzi⁹², D. Ghosh⁴⁶, S. Gieseke⁵⁴, D. Gillberg⁹³, G.F. Giudice⁵⁶, E.W.N. Glover³⁰, F. Goertz⁵⁶, D. Gonçalves³⁰, J. Gonzalez-Fraile⁴⁴, M. Gorbahn⁹⁴, S. Gori⁹⁵, C.A. Gottardo⁵⁸, M. Gouzevitch⁹⁶, P. Govoni⁹⁷, D. Gray^{29,98}, M. Grazzini³⁶, N. Greiner³⁶, A. Greljo^{36,99}, J. Grigo¹⁰⁰, A.V. Gritsan¹⁰¹, R. Gröber^{62,30}, S. Guindon¹⁰², H.E. Haber¹⁰³, C. Han¹⁰⁴, T. Han⁸⁸, R. Harlander³⁴, M.A. Harrendorf³³, H.B. Hartanto³⁴, C. Hays¹⁰⁵, S. Heinemeyer^{106,107,108}, G. Heinrich⁷⁵, M. Herrero⁴⁷, F. Herzog⁴⁵, B. Hespel⁶, V. Hirschi⁷⁴, S. Hoeche⁷⁴, S. Honeywell¹⁰⁹, S.J. Huber²⁶, C. Hugonie¹¹⁰, J. Huston¹¹¹, A. Ilnicka^{36,112}, G. Isidori³⁶, B. Jäger²⁵, M. Jaquier¹², S.P. Jones⁷⁵, A. Juste^{4,5}, S. Kallweit¹¹³, A. Kaluza¹¹⁴, A. Kardos¹¹⁵, A. Karlberg²⁰, Z. Kassabov^{116,85}, N. Kauer¹¹⁷, D.I. Kazakov^{118,33}, M. Kerner⁷⁵, W. Kilian¹¹⁹, F. Kling^{120,55}, K. Köneke¹², R. Kogler¹²¹, R. Konoplich^{29,98}, S. Kortner⁷⁵, S. Kraml¹²², C. Krause⁵⁰, F. Krauss³⁰, M. Krawczyk²², A. Kulesza¹²³, S. Kuttimalai³⁰, R. Lane¹²⁴, A. Lazopoulos¹⁹, G. Lee¹²⁵, P. Lenzi¹²⁶, I.M. Lewis¹²⁷, Y. Li⁵⁵, S. Liebler², J. Lindert³⁶, X. Liu⁶⁶, Z. Liu⁵⁵, F.J. Llanes-Estrada⁶⁹, H.E. Logan⁹³, D. Lopez-Val⁶, I. Low^{42,128}, G. Luisoni⁵⁶, P. Maierhöfer¹², E. Maina¹¹⁶, B. Mansoulié¹²⁹, H. Mantler^{53,54}, M. Mantoani¹³⁰, A.C. Marini¹³¹, V.I. Martinez Outschoorn⁵², S. Marzani¹³², D. Marzocca³⁶, A. Massironi¹³³, K. Mawatari¹²², J. Mazzitelli^{82,134}, A. McCarn¹³⁵, B. Mellado¹³⁶, K. Melnikov¹⁰⁰, S.B. Menari¹³⁷, L. Merlo⁴⁷, C. Meyer¹³⁸, P. Milenovic⁵⁶, K. Mimasu²⁶, S. Mishima¹³⁹, B. Mistlberger⁵⁶, S.-O. Moch⁹¹, A. Mohammadi¹⁴⁰, P.F. Monni²⁰, G. Montagna⁴⁰, M. Moreno Llácer¹³⁰, N. Moretti³⁶, S. Moretti¹⁵, L. Motyka¹⁴¹, A. Mück³⁴, M. Mühlleitner⁵⁴, S. Munir¹⁴², P. Musella¹¹², P. Nadolsky¹⁴³, D. Napoletano³⁰, M. Nebot⁴¹, C. Neu¹⁴⁴, M. Neubert¹¹³, R. Nevzorov^{145,146}, O. Nicrosini⁵⁷, J. Nielsen¹⁰³, K. Nikolopoulos¹⁴⁷, J.M. No²⁶, C. O'Brien¹¹⁷, T. Ohl⁷⁰, C. Oleari⁹⁷, T. Orimoto¹³³, D. Pagani⁶, C.E. Pandini⁸⁶, A. Papaefstathiou⁵⁶, A.S. Papanastasiou¹⁴⁸, G. Passarino¹¹⁶, B.D. Pecjak³⁰, M. Pelliccioni⁷, G. Perez⁵⁴, L. Perrozzi¹¹², F. Petriello^{149,42}, G. Petrisciani⁵⁶, E. Pianori²⁸, F. Piccinini⁵⁷, M. Pierini⁵⁶, A. Pilkington¹³⁷, S. Plätzer^{30,137}, T. Plehn⁴⁴, R. Podskubka⁵⁴, C.T. Potter¹⁵⁰, S. Pozzorini³⁶, K. Prokofiev^{39,151}, A. Pukhov¹⁵², I. Puljak¹⁵³, M. Queitsch-Maitland¹³⁷, J. Quevillon¹⁵⁴, D. Rathlev², M. Rauch⁵⁴, E. Re²⁷, M.N. Rebelo⁴³, D. Rebuzzi⁴⁰, L. Reina¹⁰⁹, C. Reuschle¹⁰⁹, J. Reuter², M. Riembau^{5,2}, F. Riva⁵⁶, A. Rizzi¹⁵⁵, T. Robens¹⁵⁶, R. Röntsch¹⁰⁰, J. Rojo²⁰, J.C. Romão⁴³, N. Rompotis¹⁵⁷, J. Roskes¹⁰¹, R. Roth⁵⁴, G.P. Salam⁵⁶, R. Salerno¹⁵⁸, M.O.P. Sampaio⁶⁵, R. Santos^{159,160}, V. Sanz²⁶, J.J. Sanz-Cillero⁴⁷, H. Sargsyan³⁶, U. Sarica¹⁰¹, P. Schichtel³⁰, J. Schlenk⁷⁵, T. Schmidt¹², C. Schmitt¹¹⁴, M. Schönher³⁶, U. Schubert⁷⁵, M. Schulze⁵⁶, S. Sekula¹⁴³, M. Sekulla⁵⁴,

E. Shabalina¹³⁰, H.S. Shao⁵⁶, J. Shelton⁵², C.H. Shepherd-Themistocleous¹⁶, S.Y. Shim², F. Siegert¹⁵⁶, A. Signer^{161,36}, J.P. Silva⁴³, L. Silvestrini⁶⁸, M. Sjodahl¹⁶², P. Slavich^{163,73}, M. Slawinska⁴⁵, L. Soffi¹⁶⁴, M. Spannowsky³⁰, C. Speckner¹², D.M. Sperka¹⁶⁵, M. Spira⁹², O. Stål¹⁶⁶, F. Staub⁵⁶, T. Stebel¹⁴¹, T. Stefaniak¹⁰³, M. Steinhauser¹⁰⁰, I.W. Stewart¹³¹, M.J. Strassler¹⁶⁷, J. Streicher⁵⁴, D.M. Strom¹⁵⁰, S. Su¹²⁰, X. Sun¹⁷, F.J. Tackmann², K. Tackmann², A.M. Teixeira¹⁶⁸, R. Teixeira de Lima¹³³, V. Theeuwes¹³², R. Thorne¹⁶⁹, D. Tommasini¹⁷⁰, P. Torrielli¹¹⁶, M. Tosi⁵⁶, F. Tramontano¹⁷¹, Z. Trócsányi¹¹⁵, M. Trott¹⁷², I. Tsinikos⁶, M. Ubiali¹⁴⁸, P. Vanlaer⁴⁹, W. Verkerke⁴⁵, A. Vicini⁸⁵, L. Viliani¹²⁶, E. Vryonidou⁶, D. Wackerlo¹³², C.E.M. Wagner^{173,42}, J. Wang¹⁶⁵, S. Wayand³³, G. Weiglein², C. Weiss^{2,119}, M. Wiesemann³⁶, C. Williams¹³², J. Winter¹¹¹, D. Winterbottom⁸, R. Wolf³³, M. Xiao¹⁰¹, L.L. Yang^{174,175,60}, R. Yohay¹⁰⁹, S.P.Y. Yuen¹⁷⁶, G. Zanderighi^{56,20}, M. Zaro^{72,73}, D. Zeppenfeld⁵⁴, R. Ziegler⁷³, T. Zirke⁷⁵, and J. Zupan⁹⁵

¹ International Center for Advanced Studies, UNSAM, 1650 Buenos Aires, Argentina

² DESY, 22607 Hamburg, Germany

³ Institut für Physik, Humboldt-Universität zu Berlin, 12489 Berlin, Germany

⁴ Institució Catalana de Recerca i Estudis Avançats, 08010 Barcelona, Spain

⁵ Institut de Física d'Altes Energies, Barcelona Institute of Science and Technology (BIST), 08193 Bellaterra, Barcelona, Spain

⁶ Centre for Cosmology, Particle Physics and Phenomenology (CP3), Université catholique de Louvain, 1348 Louvain-la-Neuve, Belgium

⁷ INFN Sezione di Torino, 10125 Torino, Italy

⁸ High Energy Physics Group, Blackett Lab., Imperial College, SW7 2AZ London, UK

⁹ University of California San Diego, CA 92093, USA

¹⁰ University of Toronto, Toronto, ON M5S 1A7, Canada

¹¹ TRIUMF, Vancouver, BC V6T 2A3, Canada

¹² Physikalisch-es Institut, Albert-Ludwigs-Universität Freiburg, 79104 Freiburg, Germany

¹³ LAL, Université de Paris-Sud, 91405 Orsay, France

¹⁴ University of Bristol, Bristol BS8 1TL, UK

¹⁵ School of Physics and Astronomy, University of Southampton, Highfield SO17 1BJ, UK

¹⁶ Rutherford Appleton Laboratory, Didcot OX110QX, UK

¹⁷ Institute of High Energy Physics, Beijing 100049, China

¹⁸ DAMTP, CMS, University of Cambridge, CB3 0WA Cambridge, UK

¹⁹ Institute for Theoretical Physics, Physics Department, ETH Zürich, 8093 Zurich, Switzerland

²⁰ Rudolf Peierls Centre for Theoretical Physics, University of Oxford, OX1 3NP Oxford, UK

²¹ Higgs Centre for Theoretical Physics, School of Physics and Astronomy, University of Edinburgh, EH9 3JZ Edinburgh, Scotland, UK

²² Institute of Theoretical Physics, Faculty of Physics, University of Warsaw, 02-093 Warsaw, Poland

²³ Berkeley Center for Theoretical Physics, Department of Physics, University of California, Berkeley, CA 94720, USA

²⁴ Lawrence Berkeley National Laboratory, Berkeley, CA 94720, USA

²⁵ Institute for Theoretical Physics, University of Tübingen, 72076 Tübingen, Germany

²⁶ Department of Physics and Astronomy, University of Sussex, BN1 9QH Brighton, UK

²⁷ LAPTh, Université Savoie Mont Blanc, CNRS, 74941 Annecy-le-Vieux, France

²⁸ Department of Physics, University of Warwick, CV4 7AL Warwick, UK

²⁹ Department of Physics, New York University, New York, NY 10003, USA

³⁰ Institute for Particle Physics Phenomenology, Department of Physics, Durham University, Durham DH1 3LE, UK

³¹ National Research Nuclear University MEPhI (Moscow Engineering Physics Institute), 115409 Moscow, Russia

³² Physikalisches Institut der Rheinische Friedrich-Wilhelms-Universität Bonn, 53115 Bonn, Ger-

- many
- ³³ Institut für Experimentelle Kernphysik, Karlsruhe Institute of Technology, 76128 Karlsruhe, Germany
- ³⁴ Institut für Theoretische Teilchenphysik und Kosmologie, RWTH Aachen University, 52056 Aachen, Germany
- ³⁵ University of Agder, 4604 Kristiansand, Norway
- ³⁶ Physik-Institut, Universität Zürich, 8057 Zurich, Switzerland
- ³⁷ Department of Physics, The Chinese University of Hong Kong, Shatin, Hong Kong
- ³⁸ Department of Physics, The University of Hong Kong, Hong Kong
- ³⁹ Department of Physics, The Hong Kong University of Science and Technology, Hong Kong
- ⁴⁰ Dipartimento di Fisica, Università di Pavia, and INFN, Sezione di Pavia, 27100 Pavia, Italy
- ⁴¹ Departamento de Física Teórica and IFIC, Universitat de València-CSIC, 46100 Burjassot, Spain
- ⁴² High Energy Physics Division, Argonne National Laboratory, Argonne, IL 60439, USA
- ⁴³ Departamento de Física and CFTP, Instituto Superior Técnico, Universidade de Lisboa, 1049-001 Lisboa, Portugal
- ⁴⁴ Institut für Theoretische Physik, Universität Heidelberg, 69120 Heidelberg, Germany
- ⁴⁵ Nikhef, Science Park 105, 1098 XG Amsterdam, The Netherlands
- ⁴⁶ Department of Particle Physics and Astrophysics, Weizmann Institute of Science, 7610001 Rehovot, Israel
- ⁴⁷ Departamento de Física Teórica and Instituto de Física Teórica, IFT-UAM/CSIC, Universidad Autónoma de Madrid, Cantoblanco, 28049 Madrid, Spain
- ⁴⁸ Technische Universität München, 85748 Garching, Germany
- ⁴⁹ Université Libre de Bruxelles, Service de physique des particules élémentaires, 1050 Bruxelles, Belgium
- ⁵⁰ Ludwig-Maximilians-Universität München, Fakultät für Physik, Arnold Sommerfeld Center for Theoretical Physics, 80333 München, Germany
- ⁵¹ CPPM, Université Aix-Marseille, 13288 Marseille, France
- ⁵² Department of Physics, University of Illinois at Urbana-Champaign, Urbana, IL 61801, USA
- ⁵³ Institute for Nuclear Physics, Karlsruhe Institute of Technology, 76344 Eggenstein-Leopoldshafen, Germany
- ⁵⁴ Institute for Theoretical Physics, Karlsruhe Institute of Technology, 76128 Karlsruhe, Germany
- ⁵⁵ Theoretical Physics Department, Fermilab, Batavia, IL 60510, USA
- ⁵⁶ CERN, 1211 Geneva 23, Switzerland
- ⁵⁷ INFN, Sezione di Pavia, 27100 Pavia, Italy
- ⁵⁸ Dipartimento di Fisica e Astronomia, Università di Padova and INFN, Sezione di Padova, 35131 Padova, Italy
- ⁵⁹ IPHC, Université de Strasbourg, CNRS/IN2P3, 67037 Strasbourg, France
- ⁶⁰ Center for High Energy Physics, Peking University, Beijing 100871, China
- ⁶¹ Illinois State University, Normal, IL 61790, USA
- ⁶² INFN, Sezione di Roma Tre, 00146 Roma, Italy
- ⁶³ Institut de Théorie des Phénomènes Physiques, EPFL, 1015 Lausanne, Switzerland
- ⁶⁴ ARC CoEPP, University of Melbourne, Victoria 3010, Australia
- ⁶⁵ Departamento de Física da Universidade de Aveiro and CIDMA, 3810-183 Aveiro, Portugal
- ⁶⁶ Maryland Center for Fundamental Physics, Department of Physics, University of Maryland, MD 20742, USA
- ⁶⁷ Brookhaven National Laboratory, Upton, NY 11973, USA
- ⁶⁸ INFN, Sezione di Roma, 00185 Roma, Italy
- ⁶⁹ Departamento de Física Teórica I, Universidad Complutense, 28040-Madrid. Spain
- ⁷⁰ Institut für Theoretische Physik und Astrophysik, 97074 Würzburg, Germany
- ⁷¹ Università degli Studi di Roma Tre and INFN, Sezione di Roma Tre, 00146 Roma, Italy

- 72 Sorbonne Universités, Université Pierre et Marie Curie Paris 06, LPTHE, 75005 Paris, France
 73 CNRS, UMR 7589, LPTHE, 75005, Paris France
 74 SLAC National Accelerator Laboratory, Menlo Park, CA 94025, USA
 75 Max-Planck-Institut für Physik, 80805 München, Germany
 76 LPT, UMR 8627, CNRS, Université de Paris-Sud, Université Paris-Saclay, 91405 Orsay, France
 77 SUPA, School of Physics and Astronomy, University of Glasgow, G12 8QQ Glasgow, UK
 78 Institute of Cosmos Sciences, Universitat de Barcelona, 08028 Barcelona, Spain
 79 Dipartimento di Fisica, Universit`a di Milano and INFN, Sezione di Milano, 20133 Milan, Italy
 80 New York City College of Technology, Brooklyn, NY 11201, USA
 81 The Graduate School and University Center, The City University of New York, New York, NY 10016 USA
 82 Departamento de Física, FCEyN, Universidad de Buenos Aires, Capital Federal, Argentina
 83 Department of Mathematics, Statistics, and Physics, Wichita State University, Wichita, KS 67206, USA
 84 Institute of High Energy Physics, Austrian Academy of Sciences, 1050 Wien, Austria
 85 Tif Lab, Dipartimento di Fisica, Università di Milano, and INFN, Sezione di Milano, 20133 Milano, Italy
 86 LPNHE, Université Pierre et Marie Curie and Université Paris-Diderot, 75005 Paris, France
 87 Institut Lagrange de Paris, Université Pierre et Marie Curie, 75005 Paris, France
 88 Department of Physics and Astronomy, University of Pittsburgh, Pittsburgh, PA 15260, USA
 89 INFN, Sezione di Genova, 16146 Genova, Italy
 90 Department of Physics, University of Liverpool, L69 7ZE Liverpool, UK
 91 II. Institut für Theoretische Physik, Universität Hamburg, 22761 Hamburg, Germany
 92 Paul Scherrer Institut, 5323 Villigen PSI, Switzerland
 93 Physics Department, Carleton University, Ottawa, ON K1S 5B6 Canada
 94 Department of Mathematical Sciences, University of Liverpool, L69 7ZL Liverpool, UK
 95 Department of Physics, University of Cincinnati, Cincinnati, OH 45221, USA
 96 Université de Lyon, Université Claude Bernard Lyon 1, CNRS-IN2P3, IPNL, 69622 Villeurbanne, France
 97 Università Milano-Bicocca and INFN, Sezione di Milano-Bicocca, 20126 Milano, Italy
 98 Physics Department, Manhattan College, Riverdale, New York, NY 10471, USA
 99 Faculty of Science, University of Sarajevo, 71000 Sarajevo, Bosnia and Herzegovina
 100 Institute for Theoretical Particle Physics, Karlsruhe Institute of Technology, 76128 Karlsruhe, Germany
 101 Department of Physics and Astronomy, Johns Hopkins University, Baltimore, MD 21218, USA
 102 Physics Department, SUNY Albany, Albany, NY 12222, USA
 103 Santa Cruz Institute for Particle Physics (SCIPP) and Department of Physics, University of California, Santa Cruz, CA 95064, USA
 104 Kavli IPMU (WPI), UTIAS, University of Tokyo, Kashiwa, 277-8583, Japan
 105 Department of Physics, Oxford University, OX1 3RH Oxford, UK
 106 Instituto de Física Teórica, IFT-UAM/CSIC, Universidad Autónoma de Madrid, Cantoblanco, 28049 Madrid, Spain
 107 Campus of International Excellence UAM+CSIC, Cantoblanco, 28049 Madrid, Spain
 108 Instituto de Física de Cantabria (CSIC/UC), 39005 Santander, Spain
 109 Physics Department, Florida State University, Tallahassee, FL 32306, USA
 110 LUPM, UMR 5299, CNRS, Université de Montpellier, 34095 Montpellier, France
 111 Department of Physics and Astronomy, Michigan State University, East Lansing, MI 48824, USA
 112 Institute for Particle Physics, Physics Department, ETH Zürich, 8093 Zurich, Switzerland
 113 PRISMA Cluster of Excellence, Johannes Gutenberg University, 55099 Mainz, Germany
 114 Institut für Physik, Johannes Gutenberg-Universität, 55099 Mainz, Germany

- 115 University of Debrecen and MTA-DE Particle Physics Research Group, 4002 Debrecen, Hungary
116 Dipartimento di Fisica, Università di Torino, INFN Sezione di Torino, 10125 Torino, Italy
117 Department of Physics, Royal Holloway, University of London, Egham Hill, Egham TW20 0EX,
UK
118 Bogoliubov Laboratory of Theoretical Physics, Joint Institute for Nuclear Research, 141980 Dubna,
Moscow Region, Russia
119 Department of Physics, University of Siegen, 57068 Siegen, Germany
120 Department of Physics, University of Arizona, Tucson, AZ 85721, USA
121 Institut für Experimentalphysik, Universität Hamburg, 22761 Hamburg, Germany
122 LPSC, Université Grenoble-Alpes, CNRS/IN2P3, 38026 Grenoble, France
123 Institute for Theoretical Physics, WWU Münster, 48149 Münster, Germany
124 High Energy Physics Group, Blackett Laboratory, Imperial College, SW7 2AZ London, UK
125 Physics Department, Technion, Haifa 32000, Israel
126 Università and INFN, Sezione di Firenze, 50019 Firenze, Italy
127 Department of Physics and Astronomy, University of Kansas, Lawrence, KS 66045, USA
128 Department of Physics and Astronomy, Northwestern University, Evanston, IL 60208, USA
129 CEA IRFU-SPP, 91191 Gif-sur-Yvette, France
130 II.Physikalisches Institut Universität Goettingen 37077 Germany
131 CTP, MIT, Cambridge, MA 02139, USA
132 Department of Physics, University at Buffalo, The State University of New York, Buffalo, NY
14260, USA
133 Department of Physics, Northeastern University, Boston, MA 02115, USA
134 International Center for Advanced Studies, UNSAM, 1650 Buenos Aires, Argentina
135 Department of Physics, The University of Michigan, Ann Arbor, MI 48104, USA
136 University of the Witwatersrand, School of Physics, Private Bag 3, Wits 2050, South Africa
137 School of Physics and Astronomy, University of Manchester, Manchester, M13 9PL, UK
138 Department of Physics, University of Pennsylvania, Philadelphia, PA 19104, USA
139 Theory Center, Institute of Particle and Nuclear Studies, KEK, Tsukuba, 305-0801, Japan
140 Kansas State University, Manhattan, KS, 66506, USA
141 M. Smoluchowski Institute of Physics, Jagiellonian University, Krakow, 30-348 Poland
142 KIAS, Seoul 130-722, Republic of Korea
143 Department of Physics, Southern Methodist University, Dallas, TX 75275, USA
144 University of Virginia, Charlottesville, VA 22903, USA
145 ARC Centre of Excellence for Particle Physics at the Terascale and CSSM, Department of Physics,
The University of Adelaide, Adelaide SA 5005, Australia
146 Institute for Theoretical and Experimental Physics, Moscow 117218, Russia
147 University of Birmingham, Birmingham B15 2TT, UK
148 University of Cambridge, The Cavendish Laboratory, CB3 0HE Cambridge, UK
149 Department of Physics and Astronomy, Northwestern University, Evanston, IL 60208, USA
150 Center for High Energy Physics, University of Oregon, Eugene, OR 97403, USA
151 HKUST Jockey Club Institute for Advanced Study, Hong-Kong
152 Lomonosov Moscow State University, Skobeltsyn Institute of Nuclear, Moscow 119992, Russia
153 University of Split, 21000 Split, Croatia
154 King's College London, WC2R 2LS London, UK
155 Dipartimento di Fisica Università di Pisa, and INFN, Sezione di Pisa, 56100 Pisa, Italy
156 Institut für Kern- und Teilchenphysik, TU Dresden, 01069 Dresden, Germany
157 University of Washington, Physics Department, Seattle WA 98195, USA
158 LLR, IN2P3-CNRS, École Polytechnique, 91128 Palaiseau, France
159 ISEL - Instituto Superior de Engenharia de Lisboa, Instituto Politécnico de Lisboa, 1959-007
Lisboa, Portugal

-
- ¹⁶⁰ Centro de Física Teórica e Computacional, Faculdade de Ciências, Universidade de Lisboa, 1749-016 Lisboa, Portugal
¹⁶¹ Paul Scherrer Institut, 5232 Villigen PSI, Switzerland
¹⁶² Department of Astronomy and Theoretical Physics, Lund University, 22362 Lund, Sweden
¹⁶³ Sorbonne Universités, UPMC Univ. Paris 06, LPTHE, 75005 Paris, France
¹⁶⁴ Cornell University, Ithaca, NY 14850, USA
¹⁶⁵ University of Florida, Gainesville, FL 32611, USA
¹⁶⁶ The Oskar Klein Centre, Department of Physics, Stockholm University, 106 91 Stockholm, Sweden
¹⁶⁷ Department of Physics, Harvard University, Cambridge, MA 02138, USA
¹⁶⁸ LPC, CNRS/IN2P3 UMR 6533, 63171 Aubière, France
¹⁶⁹ University College London, WC 1E 6BT London, UK
¹⁷⁰ Institute of Nuclear and Particle Physics, NCSR Demokritos, 15310 Agia Paraskevi, Greece
¹⁷¹ Dipartimento di Fisica "E. Pancini", Università di Napoli Federico II and INFN, Sezione di Napoli, 80126 Napoli, Italy
¹⁷² Niels Bohr International Academy, University of Copenhagen, Blegdamsvej 17, 2100 Copenhagen, Denmark
¹⁷³ Enrico Fermi Institute, Kavli Institute for Cosmological Physics, University of Chicago, Chicago, IL 60637, USA
¹⁷⁴ School of Physics and State Key Laboratory of Nuclear Physics and Technology, Peking University, Beijing 100871, China
¹⁷⁵ Collaborative Innovation Center of Quantum Matter, Beijing 100084, China
¹⁷⁶ Physikalisches Institut der Universität Bonn, 53115 Bonn, Germany

Contents

Introduction	1
I Standard Model Predictions	3
I.1 Standard Model Parameters	5
I.1.1 Lepton masses	5
I.1.2 Electroweak parameters	5
I.1.3 QCD parameters and parton densities	5
I.1.3.a Strong coupling constant	6
I.1.3.b Quark masses	6
I.1.4 Higgs boson mass	7
I.2 Parton Distribution Functions	9
I.2.1 The PDF4LHC recommendation	9
I.2.2 The PDF4LHC15 PDF sets	11
I.2.3 Higgs boson production cross-sections	13
I.2.4 Strong coupling and heavy quark masses	13
I.2.5 PDF correlations	17
I.2.6 Acceptance calculations	18
I.2.7 Summary	19
I.3 Branching Ratios	21
I.3.1 Update of branching ratios and decay width for the Standard Model Higgs boson	21
I.3.1.a Strategy and input for branching-ratio calculations	21
I.3.1.b Partial widths and BR for Higgs boson masses close to 125 GeV	23
I.3.1.c Correlations and uncertainties for BR close to 125 GeV	25
I.3.1.d Partial widths and BR for a wide Higgs boson mass range	25
I.3.1.e HTO4L : a generator for Higgs boson decay into four charged leptons	26
I.3.2 Update on MSSM branching ratios	27
I.4 Gluon-gluon Fusion	29
I.4.1 The inclusive cross-section	29
I.4.1.a The N^3LO cross section	29
I.4.1.b N^3LL resummation	34
I.4.1.c Combined fixed order and resummed results at N^3LO+N^3LL	37
I.4.1.d Summary for the total cross-section	43
I.4.2 Differential and jet-binned cross sections	45
I.4.2.a General treatment of theory uncertainties in kinematic bins	46
I.4.2.b Exclusive fixed-order cross sections and jet-veto efficiencies at $NNLO$	49
I.4.2.c Combined resummed predictions for the 0-jet, 1-jet, and ≥ 2 -jet bins	55
I.4.2.d Jet-vetoed Higgs cross section in gluon fusion at $N^3LO+NNLL$	62

I.4.2.e	Higgs- p_T resummation in momentum space at NNLL+NNLO in gluon fusion	66
I.4.2.f	NNLOJET: $H + j$ at NNLO using Antenna subtraction	69
I.4.3	Benchmarks for cross sections and differential distributions	70
I.4.3.a	Calculations and codes	71
I.4.3.b	Observables	73
I.4.4	Effects of heavy-quark masses	78
I.4.4.a	Implementation of quark mass corrections	79
I.4.4.b	Finite top mass effects	80
I.4.4.c	Nonzero bottom mass effects	81
I.4.4.d	Conclusions	83
I.5	VBF and VH	85
I.5.1	VBF cross-section predictions	85
I.5.1.a	Programs and tools for VBF	85
I.5.1.b	VBF parameters and cuts	87
I.5.1.c	Integrated VBF cross sections	88
I.5.1.d	Differential VBF cross sections	90
I.5.2	VH cross-section predictions	93
I.5.2.a	Programs and tools for VH	93
I.5.2.b	VH parameters and cuts	95
I.5.2.c	Total VH cross sections	96
I.5.2.d	Fiducial and differential VH cross sections	99
I.5.2.e	Cross-section predictions including the decay $H \rightarrow b\bar{b}$	101
I.5.3	Electroweak production of H+3jets at NLO+PS	107
I.5.4	VH production at NLO+PS	109
I.5.5	NNLOPS for VH	113
I.6	ttH and tH	121
I.6.1	Introduction	121
I.6.2	NLO QCD+EW predictions for $t\bar{t}H$ production	121
I.6.3	Comparison of NLO QCD+Parton Shower simulations for $t\bar{t}H(b\bar{b})$	123
I.6.4	Off-shell effects in $t\bar{t}H$ production	127
I.6.4.a	$t\bar{t}H$ with off-shell top decays: $W^+W^-b\bar{b}H$ production at NLO QCD	127
I.6.4.b	Background and interference effects: $\ell\nu + jj + b\bar{b}b\bar{b}$ production at LO QCD	137
I.6.5	$t\bar{t}H$ production beyond NLO	142
I.6.5.a	NLO+NLL soft-gluon resummation in the partonic centre-of-mass threshold limit	143
I.6.5.b	Approximate NNLO via soft-gluon resummation in the ‘‘PIM’’ limit	146
I.6.6	tH production at NLO in QCD	151
I.6.6.a	t -channel tH production	151
I.6.6.b	s -channel tH production	155
I.6.7	$t\bar{t}Z$ and $t\bar{t}W^\pm$ production	156
I.6.7.a	NLO QCD+EW predictions for $t\bar{t}Z$ and $t\bar{t}W^\pm$ production	156
I.6.7.b	Comparison of NLO QCD predictions for differential distributions	161
I.6.7.c	$t\bar{t}VV$ production ($V = Z, W^\pm, H$) at NLO QCD	163
I.6.8	NLO+PS simulations of $t\bar{t}b\bar{b}$ production	170
I.6.8.a	NLO+PS tools and simulations	171
I.6.8.b	Parton showers, PDF, and α_s	172
I.6.8.c	Input parameters and scale choices	173
I.6.8.d	NLO+PS predictions for $t\bar{t} + b$ -jets cross sections in b -jet bins	174
I.6.8.e	ttb differential analysis	175

I.6.8.f	ttbb differential analysis	175
I.6.8.g	Summary and conclusions	176
I.7 Higgs Boson Pair Production		187
I.7.1	Introduction	187
I.7.2	Total rates in the SM	188
I.7.2.a	Gluon fusion	188
I.7.2.b	Other production channels	191
I.7.3	Differential distributions	195
I.7.4	Benchmark BSM scenarios	199
I.7.4.a	Effective Field Theory	199
I.7.4.b	Higgs Singlet Model	202
I.7.4.c	2 Higgs Doublet Model	204
I.7.5	Experimental results	218
I.8 Off-shell Higgs Production and Higgs Interference		221
I.8.1	Introduction	221
I.8.2	Overview	222
I.8.3	$H \rightarrow VV$ modes ($V = W, Z$)	222
I.8.3.a	Input parameters and recommendations for input parameters and PDF	222
I.8.3.b	Off-shell and interference benchmarks: Standard Model	223
I.8.3.c	Off-shell and interference benchmarks: 1-Higgs Singlet Model	229
I.8.3.d	Multijet merging effects in $gg \rightarrow \ell\bar{\nu}_\ell \ell'\bar{\nu}_{\ell'}$ using SHERPA	234
I.8.3.e	Study of higher-order QCD corrections in the $gg \rightarrow H \rightarrow VV$ process	238
I.8.3.f	Higgs boson off-shell simulation with the MCFM and JHU generator frameworks	244
I.8.3.g	Interference contributions to heavy Higgs boson production in the 2HDM	246
I.8.4	$gg \rightarrow VV$ at NLO QCD	252
I.8.4.a	The status of theoretical predictions	252
I.8.4.b	Brief description of the NLO computation for $gg \rightarrow 4l$	253
I.8.4.c	Results and recommendation for the $gg (\rightarrow H) \rightarrow ZZ$ interference K -factor	255
I.8.5	$H \rightarrow \gamma\gamma$ mode	257
I.8.5.a	Theory overview	258
I.8.5.b	Monte Carlo interference implementations	264
I.8.5.c	Studies from ATLAS	266
I.9 Summary		273
II Effective Field Theory Predictions		277
II.1 Executive Summary of Parts II and III		279
II.2 EFT Formalism		283
II.2.1	Bases for the Standard Model Effective Field Theory	283
II.2.1.a	Introduction	283
II.2.1.b	SM EFT with dimension-6 operators	284
II.2.1.c	Effective Lagrangian of mass eigenstates	286
II.2.1.d	Higgs basis	295
II.2.2	Comments on the validity of the EFT approach to physics beyond the SM	303
II.2.2.a	Introduction	303
II.2.2.b	General discussion	304

II.2.2.c	Model-independent experimental results	304
II.2.2.d	EFT validity and interpretation of the results	305
II.2.2.e	On the importance of loop corrections	307
II.2.2.f	An Explicit Example	307
II.2.2.g	Summary	310
II.2.3	The Standard Model EFT and Next to Leading Order	311
II.2.3.a	Overview	311
II.2.3.b	Introduction to the SMEFT	312
II.2.3.c	Known results in the SMEFT to NLO	333
II.2.3.d	Summary and comments	336
II.2.4	Non-linear EFT	339
II.2.4.a	Motivation and leading-order Lagrangian	339
II.2.4.b	Renormalization of the chiral Lagrangian	342
II.2.4.c	Connection of chiral Lagrangian to κ -formalism	343
II.2.4.d	Linear vs. nonlinear EFT	345
II.2.4.e	Sample applications	346
II.2.4.f	Concluding remarks	353
II.2.5	Fitting EFT parameters and constraining models	353
II.2.5.a	The problem	353
II.2.5.b	Measuring dimension-6 Wilson coefficients	354
II.2.5.c	Weakly interacting new physics to dimension-6	359
II.3	EFT Application	371
II.3.1	High-energy physics tools for the study of the Higgs boson properties in EFT	371
II.3.1.a	Introduction	371
II.3.1.b	HiGlu: Higgs boson production via gluon fusion	372
II.3.1.c	Hawk: vector boson fusion and Higgs-strahlung channels	374
II.3.1.d	HPair: Higgs boson pair production via gluon fusion	375
II.3.1.e	eHDecay, Higgs boson decays in the effective Lagrangian approach	376
II.3.1.f	Higgs Pseudo-Observables in the universal FeynRules output	378
II.3.1.g	Higgs and BSM characterization in the MG5_aMC@NLO framework	380
II.3.1.h	Higgs boson properties with the JhuGen / Mela framework	384
II.3.1.i	Higgs boson pair production in HERWIG 7	385
II.3.1.j	Anomalous couplings in VBFNLO	386
II.3.1.k	Event generation with Whizard	388
II.3.1.l	Constraints on non-standard Higgs boson couplings with HEPfit	390
II.3.1.m	Rosetta	390
II.3.2	Morphing implementation	392
II.3.2.a	Morphing principles	393
II.3.2.b	General procedure to construct morphing function	393
II.3.2.c	Conclusions	396
III	Measurements and Observables	397
III.1	Pseudo-observables	399
III.1.1	Introduction	399
III.1.2	Two-body decay modes	400
III.1.2.a	$h \rightarrow f\bar{f}$	400
III.1.2.b	$h \rightarrow \gamma\gamma$	401

III.1.3 Three-body decay modes	402
III.1.3.a $h \rightarrow f\bar{f}\gamma$	402
III.1.4 Four-fermion decay modes	404
III.1.4.a $h \rightarrow 4f$ neutral currents	404
III.1.4.b $h \rightarrow 4f$ charged currents	405
III.1.4.c $h \rightarrow 4f$ complete decomposition	406
III.1.4.d <i>Physical PO</i> for $h \rightarrow 4\ell$	406
III.1.4.e <i>Physical PO</i> for $h \rightarrow 2\ell 2\nu$	408
III.1.5 PO in Higgs electroweak production: generalities	409
III.1.5.a Amplitude decomposition	410
III.1.6 PO in Higgs electroweak production: phenomenology	413
III.1.6.a Vector Boson Fusion	413
III.1.6.b Associated vector boson plus Higgs boson production	415
III.1.6.c Validity of the momentum expansion	416
III.1.6.d Illustration of NLO QCD effects	417
III.1.7 Parameter counting and symmetry limits	418
III.1.7.a Yukawa modes	418
III.1.7.b Higgs EW decays	419
III.1.7.c EW production processes	419
III.1.7.d Additional PO	420
III.1.8 PO meet SMEFT	421
III.1.8.a SMEFT summary	422
III.1.8.b Theoretical uncertainty	423
III.1.8.c Examples	424
III.1.8.d SMEFT and <i>physical PO</i>	431
III.1.8.e Summary on the PO-SMEFT matching	433
III.1.9 Conclusions	433
III.2 Simplified Template Cross Sections	437
III.2.1 Overview	437
III.2.2 Guiding principles in the definition of simplified template cross section bins	439
III.2.2.a Splitting of production modes	440
III.2.2.b Staging	440
III.2.3 Definition of leptons and jets	441
III.2.3.a Higgs boson	441
III.2.3.b Leptons	441
III.2.3.c Jets	442
III.2.4 Bin definitions for the different production modes	442
III.2.4.a Bins for $gg \rightarrow H$ production	442
III.2.4.b Bins for VBF production	444
III.2.4.c Bins for VH production	445
III.2.4.d Treatment of $t\bar{t}H$ production	448
III.2.4.e Treatment of $b\bar{b}H$ and tH production	448
III.2.5 Practical considerations	448
III.2.6 Summary	448
III.3 Higgs Fiducial Cross Sections	449
III.3.1 Introduction	449
III.3.2 Review of Run 1 and early Run 2 results	450
III.3.3 State-of-the-art Standard Model predictions	453

III.3.3.a	Template fiducial regions for benchmark	454
III.3.3.b	Fiducial cross sections for Higgs boson production in association with $n_{\text{jet}} \geq 1$ jets	455
III.3.3.c	Fiducial cross sections for Higgs boson production in association with $n_{\text{jet}} \geq 1$ jets	458
III.3.3.d	Fiducial cross section and distribution for the irreducible background	461
III.3.3.e	QCD activity associated with Higgs production in gluon fusion	464
III.3.4	Beyond the Standard Model effects	468
III.3.4.a	Higgs boson production in gluon fusion	468
III.3.4.b	Boosted Higgs boson production in gluon fusion	470
III.3.4.c	VH associated production	470
III.3.4.d	Vector boson fusion	471
III.3.4.e	Invisible Higgs boson decays	472
III.3.4.f	Mono-Higgs signatures	473
III.3.5	Experimental aspects	473
III.3.5.a	Definition of the fiducial phase space	473
III.3.5.b	Unfolding of experimental data	476
III.3.5.c	Model dependence	478
III.3.5.d	Treatment of the Higgs boson mass in fiducial and differential measurements	479
III.3.5.e	Combination of inclusive cross sections for Higgs boson production	480
III.3.6	Summary and recommendations for future measurements	482
IV	Beyond the Standard Model Predictions	485
IV.1	Neutral MSSM	487
IV.1.1	Introduction	487
IV.1.2	Benchmark scenarios for low $\tan \beta$ in the MSSM	490
IV.1.2.a	The hMSSM approach	491
IV.1.2.b	The “low-tb-high” scenario	493
IV.1.3	ROOT files for cross sections and branching ratios	495
IV.1.3.a	Content of the ROOT files	495
IV.1.3.b	Technical details and data access	497
IV.1.3.c	Comparison of benchmark scenarios for low $\tan \beta$	498
IV.1.4	Description of the transverse momentum of the Higgs boson in gluon fusion	502
IV.1.4.a	Determination of the matching scale	502
IV.1.4.b	Resummation frameworks	504
IV.1.4.c	Phenomenological analysis in the THDM	504
IV.2	Neutral Higgs Boson Production in Association with Bottom Quarks	509
IV.2.1	Introduction	509
IV.2.2	Total inclusive cross section	511
IV.2.2.a	Choice of bottom PDFs in the 5FS	512
IV.2.2.b	Santander matching	514
IV.2.2.c	NLO+NLL matching	515
IV.2.2.d	FONLL matching	519
IV.2.2.e	Comparison of different matching approaches	520
IV.2.3	Differential Monte-Carlo predictions	522
IV.2.3.a	$b\bar{b}\phi$ in MG5_aMC@NLO	522
IV.2.3.b	$b\bar{b}\phi$ in the POWHEG BOX	524

IV.2.3.c	$b\bar{b}\phi$ in SHERPA	525
IV.2.3.d	Comparison of the Monte-Carlo tools	526
IV.2.3.e	Recommendations for $b\bar{b}\phi$ signal simulation	529
IV.2.4	Acceptance uncertainties	531
IV.2.5	Total cross sections for $c\bar{c}\phi$ production	532
IV.3	Charged Higgs Bosons	535
IV.3.1	Introduction	535
IV.3.2	Inclusive production cross sections	535
IV.3.3	Differential production cross sections	539
IV.3.4	Recommendations for signal simulation	544
IV.4	Extended Scalar Sector	545
IV.4.1	Introduction	545
IV.4.1.a	Input parameters	548
IV.4.2	Tools and constraints	549
IV.4.2.a	Vacuum stability and theoretical constraints	549
IV.4.2.b	Experimental constraints	549
IV.4.2.c	Calculation of cross sections and decay widths	550
IV.4.3	Benchmark points	550
IV.4.3.a	Benchmark points <i>BP1</i>	551
IV.4.3.b	Benchmark points <i>BP2</i>	555
IV.4.3.c	Benchmark points <i>BP3</i>	557
IV.4.3.d	Benchmark points <i>BP4</i>	558
IV.4.3.e	Benchmark points <i>BP5</i>	560
IV.4.3.f	Benchmark points <i>BP6</i>	564
IV.4.3.g	Benchmark points <i>BP7</i>	564
IV.4.3.h	Benchmark points <i>BP8</i>	570
IV.4.4	Georgi-Machacek model	571
IV.4.4.a	Model parameterization	572
IV.4.4.b	H ₅ plane benchmark	575
IV.4.4.c	Vector boson fusion production cross sections of the H ₅ states	576
IV.4.4.d	Decay widths of the H ₅ states	577
IV.4.5	Singlet	584
IV.4.5.a	Introduction	584
IV.4.5.b	Tools	587
IV.4.5.c	Benchmarks	587
IV.4.5.d	Benchmark points for the CxSM and RxSM	588
IV.5	NMSSM	601
IV.5.1	Introduction	601
IV.5.2	Tools for the NMSSM	602
IV.5.2.a	Calculation of the spectrum and of the branching fractions	602
IV.5.2.b	Check for the vacuum stability	605
IV.5.2.c	Calculation of the neutral Higgs boson production cross sections	605
IV.5.3	NMSSM benchmark points	607
IV.5.3.a	NMSSM specific processes	607
IV.5.3.b	Benchmark points	610
IV.6	Exotic Higgs Decays	619
IV.6.1	Introduction and motivation	619

IV.6.2 Exclusive mesonic and flavour-violating Higgs boson decays	620
IV.6.2.a Theoretical predictions: photon plus a meson	620
IV.6.2.b $h \rightarrow VP$ and $h \rightarrow VP^*$	625
IV.6.2.c NP benchmarks for enhanced branching ratios	627
IV.6.2.d Experimental status and prospects	637
IV.6.3 Recommendations for searches for exotic Higgs boson decays	640
IV.6.4 Partonic distributions for the prompt decay topology $h \rightarrow XX \rightarrow 2Y2Y'$	641
IV.6.4.a Introduction	641
IV.6.4.b Signal model and event generation	642
IV.6.4.c Results	643
IV.6.5 Prospects for prompt decays with MET: $h \rightarrow 2\gamma + \cancel{E}_T$ test case	646
IV.6.5.a Introduction	646
IV.6.5.b Methodology	647
IV.6.5.c Results	651
IV.6.6 Long lived particles from Higgs boson decays	653
IV.6.6.a Overview and motivation	653
IV.6.6.b Displaced objects	654
IV.6.6.c Higgs boson decays to displaced photons and missing energy from Supersymmetry	663
 Acknowledgements	 665
 Appendices	 673
A Tables of branching ratios	675
B SM gluon-gluon-fusion cross sections	689
C SM vector-boson-fusion cross sections	697
D SM Higgs-strahlung cross sections	713
E $t\bar{t}H$ and tH cross sections	735
F $b\bar{b}H$ cross sections	753
 References	 761

Chapter I.2

Parton Distribution Functions

S. Forte, J. Huston, R. S. Thorne (Eds.); S. Carrazza, J. Gao, Z. Kassabov, P. Nadolsky, J. Rojo

I.2.1 The PDF4LHC recommendation

Previous Yellow Reports [7–9] have provided snapshots of the state-of-the-art for PDF determination, along with recommendations for PDF use, and for calculations of PDF uncertainties, following the guidance of the PDF4LHC group. In a previous recommendation [28], three PDF sets were used: CT10 [29], MSTW2008 [30] and NNPDF2.3 [31]. These were global PDF fits involving data from a variety of experiments, including collider data from the Tevatron. The uncertainty was provided by the envelope of all three PDF error sets, and the central prediction as mid-point of this envelope. This choice is conservative but not ideal, in that it tends to be dominated by error PDFs at the edge of the uncertainty band; it was adopted because it was felt that the degree of agreement of the PDF sets was not sufficient to warrant their statistical combination. Specifically, agreement was unsatisfactory for the gluon distribution, particularly in the region appropriate for Higgs boson production through gluon-gluon fusion. This disagreement prompted an intensive year-long study by the three global PDF groups, along with HERAPDF [32], but this did not uncover a clear explanation for the differences [33].

Prior to the writing of YR4, the major PDF groups have released updates to their PDF fits, at NLO and NNLO, including in most cases data from the LHC [34]. The new PDF4LHC recommendation [35] uses the updated PDFs from the three global PDF groups included in the previous recommendation: CT14 [36], MMHT14 [37] and NNPDF3.0 [38], respectively. Details as to why this choice was made can be found in the PDF4LHC document. The primary requirements are that the PDFs should be based on global datasets, be carried out in a general-mass variable flavour-number scheme, and have compatible values for the QCD coupling constant $\alpha_s(m_Z)$. As we shall see shortly, these new PDF sets are in good agreement, not only in the quark sector (where the agreement was satisfactory already in the previous generation of PDFs) but also for the gluon. The changes can be ascribed partially to the addition of new data sets used in the PDF fits, but primarily to improvements in the fitting formalisms. This level of agreement may change in detail with future updates, but generally the good level of agreement should stay. An alternative recommendation [39] is that all PDFs (ABM12 [40], CJ15 [41], CT14 [36], HERAPDF2.0 [32], JR14 [42], HERAPDF2.0 [32] MMHT14 [37], NNPDF3.0 [38]) and accompanying coupling and quark mass variation should be used for precision theory predictions and any LHAPDF6 [43] PDF set for other predictions.

Currently, there are two different representations of PDF uncertainties: the Monte Carlo representation [44, 45] and the Hessian representation [46]. Both provide compatible descriptions of the PDF uncertainties, and recent developments have allowed for the straight-forward conversion of one representation to the other [47–49]. The use of the Monte Carlo representation makes possible a statistical combination of different PDF sets. If different PDF sets can be assured to be equally likely representations of the underlying PDF probability distribution, they can be combined simply by taking their un-weighted average. This can be arrived at by generating equal numbers of Monte Carlo replicas from each input PDF set, and then merging the replica sets. The NNPDF3.0 PDF set is naturally in this format. For the Hessian sets, CT14 and MMHT2014, the Monte Carlo replicas are generated by sampling along the eigenvector directions, assuming a Gaussian distribution.

Combinations in this manner are most appropriate when the PDF sets that are combined are compatible with each other, as CT14, MMHT2014 and NNPDF3.0 are. Such a combination also allows for a direct statistical interpretation of the resulting PDF uncertainties, unlike the envelope method. Monte

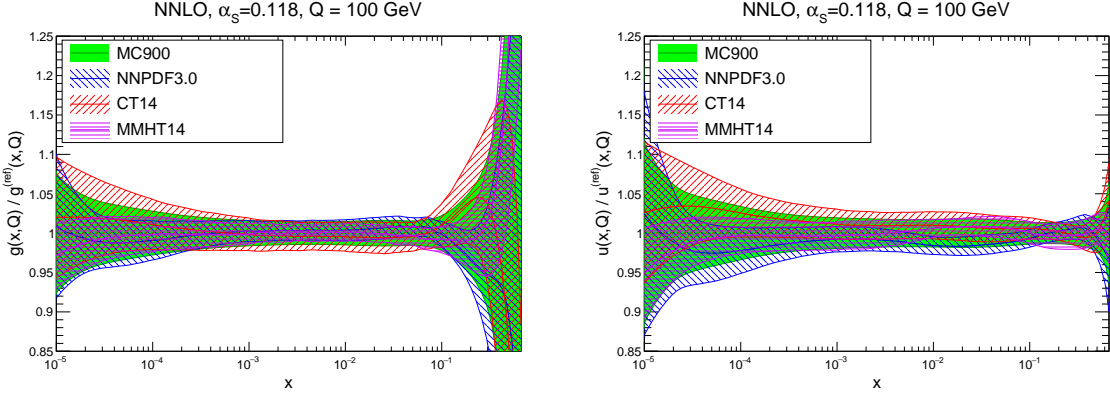


Figure 2: Comparison of the MC900 PDFs with the sets that enter the combination: CT14, MMHT14 and NNPDF3.0 at NNLO. We show the gluon and the up quark at $Q = 100$ GeV. Results are normalized to the central value of the prior set MC900.

Carlo combinations of these three PDFs have been provided at both NLO and NNLO by the PDF4LHC working group. In the following discussion we concentrate on NNLO; similar considerations apply to NLO.

It was determined that $N_{\text{rep}} = 900$ Monte Carlo replicas, combining $N_{\text{rep}} = 300$ replicas from each of the three individual PDF sets, were sufficient to represent the combined PDF probability distribution. In Figure 2 we show a comparison of the combined PDF4LHC15 NNLO set (indicated by MC900 in the plot) with the three sets that enter the combination, CT14, MMHT14 and NNPDF3.0. We show the gluon and the up quark at $Q = 100$ GeV, normalized to the central value of the PDF4LHC15 combination. In these plots, as in the rest of this chapter, we use a fixed value $\alpha_s(m_Z) = 0.118$.

It can be seen that in the “precision physics” region, roughly from $x \simeq 0.001$ to $x \simeq 0.1$, the PDFs from the three global sets agree reasonably well with each other, with perfect agreement for the gluon, and less good agreement for the up quark. This is reflected in the combined PDF4LHC15 set, constructed from the three input PDF sets. On the other hand, at low and high values of x , the uncertainty bands from the three PDF sets differ, and the uncertainty band for the 900 Monte Carlo replicas is smaller than the envelope of the three PDF uncertainty bands. These are regions in which PDFs are only weakly constrained by data, as seen by the increasingly large size of the uncertainty, and the inflated uncertainty in the combination appears to provide a reasonable estimate.

In Figure 3 we compare the NNLO PDF luminosities at the LHC 13 TeV computed using the prior set PDF4LHC15 NNLO, both to the three sets which were used for the previous PDF4LHC recommendation (CT10, MSTW08 and NNPDF2.3), and the three sets which enter the current combination CT14, MMHT14 and NNPDF3.0 NNLO. We show the gg and $q\bar{q}$ luminosities as a function of the invariant mass of the final state M_X , normalized to the central value of PDF4LHC15_nnlo_prior. The improvement in compatibility of the new sets in comparison to the old ones, especially in the gluon sector, is apparent, particularly in the precision mass region, say roughly 50 GeV to 1 TeV (more so for gg than for $q\bar{q}$). Reassuringly, even though uncertainty estimates differ somewhat between current sets, especially for quarks, central values of all sets in this region are in good agreement. Interestingly, they also agree well with the mid-point of the envelope of the old sets. Hence, in practice, in the precision region, the central prediction with the old prescription (the envelope of CT10, MSTW08, and NNPDF2.3) and the new prescription (the PDF4LHC15 combined set) are actually quite close.

There is more disagreement in the low mass region and in the high mass region, and the range of uncertainty for the 900 set Monte Carlo can be less than the envelope of the three PDF groups. This is not surprising, as the combined uncertainty band reflects the common trend of all input PDF ensembles, while the envelope unduly emphasizes extreme behaviour of a few replicas. While the combined

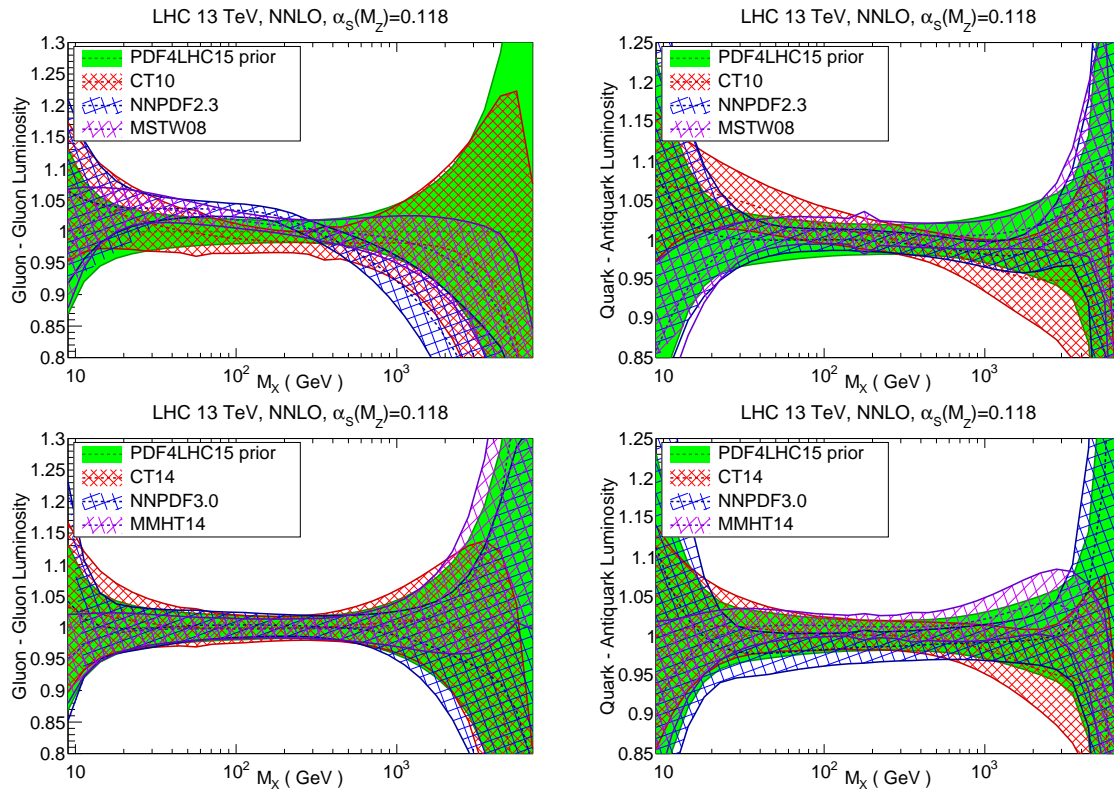


Figure 3: Comparison of NNLO parton luminosities at the LHC 13 TeV. Top: the PDF4LHC15 combined set compared to the CT10, MSTW08, and NNPDF2.3 PDF set whose envelope was used as a previous PDF4LHC recommendation. Bottom: the PDF4LHC15 combined set compared to the three individual sets which enter the combination: CT14, MMHT14 and NNPDF3.0. The gg (left) and the $q\bar{q}$ (right) luminosities are shown as a function of the invariant mass of the final state M_X , normalized to the central value of PDF4LHC15_nnlo_prior.

uncertainty appears to be conservative enough, this should be kept in mind especially in discussions of uncertainties of high-mass searches.

I.2.2 The PDF4LHC15 PDF sets

Although the $N_{\text{rep}} = 900$ Monte Carlo set itself could be used to determine PDF uncertainties for any LHC process, it suffers from the drawback of having a very large number of PDFs in the set; also, for many applications the non-Hessian framework may be a further drawback. However, the most essential features of the PDF uncertainties can be captured using three techniques that significantly reduce the number of error PDFs needed, especially in view of the fact that there is an uncertainty in the determination of the PDF uncertainties (witness the differences between the PDF groups at low x and high x), and therefore very high precision is not justified in view of the limited accuracy.

Two of these techniques use the Hessian formalism, considering only symmetric PDF uncertainties, while the third technique uses a compressed Monte Carlo technique, which allows for asymmetric uncertainties. Details of the derivations are provided in the PDF4LHC document. Correspondingly, three delivery options are available for the combined sets:

- PDF4LHC15_mc: contains 100 PDFs, including non-Gaussian features, constructed using the CMC method [50].
- PDF4LHC15_30: contains 30 PDFs in a Hessian framework, determined using the META-PDF technique [48].
- PDF4LHC15_100: contains 100 PDFs in a Hessian framework, determined using the MC2H approach [49].

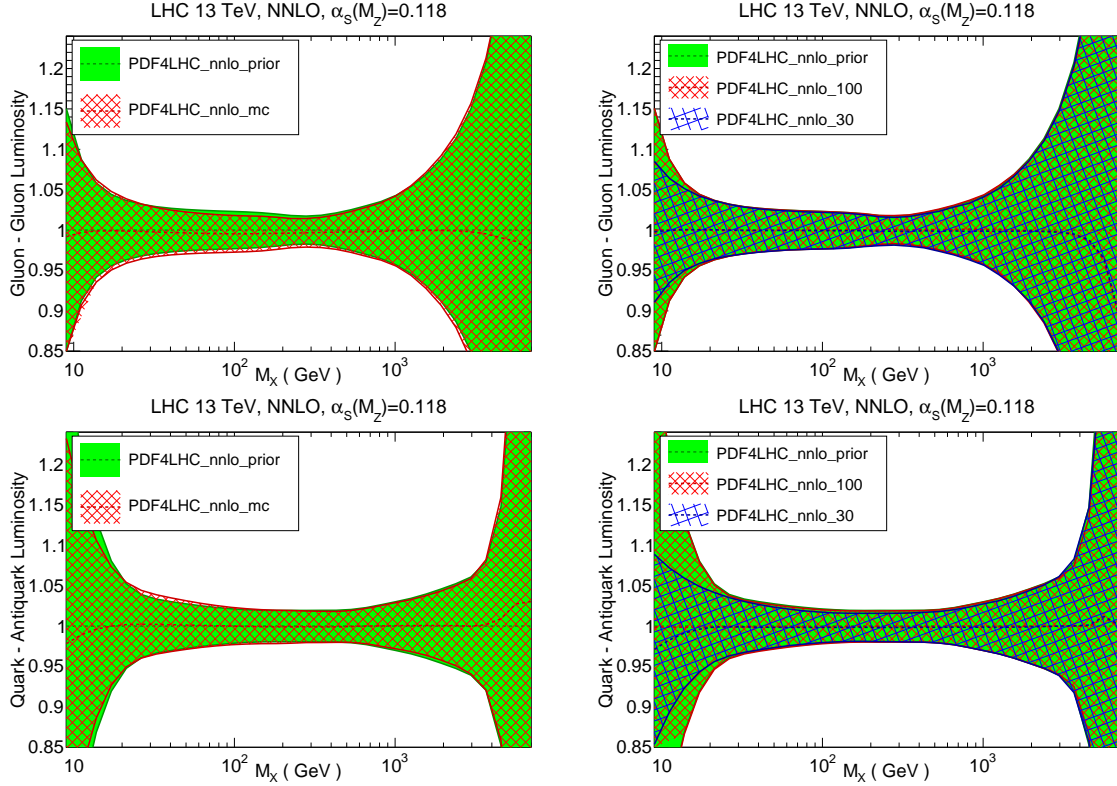


Figure 4: Comparison of parton luminosities at the LHC 13 TeV computed using the prior set PDF4LHC15_nnlo_prior with its compressed Monte Carlo representation, PDF4LHC15_nnlo_mc (left plots) and with its two Hessian sets, PDF4LHC15_nnlo_100 and PDF4LHC15_nnlo_30. We show the gg (upper plots) and $q\bar{q}$ (lower plots) luminosities as a function of the invariant mass of the final state M_X , normalized to the central value of PDF4LHC15_nnlo_prior.

We will henceforth refer to the starting 900 replica Monte Carlo set as the “prior”, from which these reduced sets are constructed: PDF4LHC15_nnlo_prior.

A central value of $\alpha_s(m_Z) = 0.118$ is used for each of these sets, at both NLO and NNLO, with an uncertainty of $\delta\alpha_s(m_Z) = 0.0015$ as recommended in the chapter on Standard Model parameters of this document. Therefore, for each option, individual error sets using $\alpha_s(m_Z) = 0.1165$ and 0.1195 are provided in order to be able to compute the uncertainty due to $\delta\alpha_s(m_Z)$ in LHC cross-sections, which should be added in quadrature with the PDF uncertainty [35]. It has been verified that addition in quadrature is a good enough approximation (in some cases exact) to the exact recipes for PDF and α_s combination provided by each group [51–53].

The gluon-gluon and quark-antiquark PDF luminosities as a function of the final-state invariant mass M_X at the LHC 13 TeV are shown in Figure 4, where we compare the prior set PDF4LHC15_nnlo_prior with its compressed Monte Carlo representation, PDF4LHC15_nnlo_mc and with the two Hessian reduced sets, PDF4LHC15_nnlo_100 and PDF4LHC15_nnlo_30. Note that by construction the central values of the two Hessian reduced sets coincide with the central value of the prior, while the central value of the Monte Carlo set reproduces it within the precision of the compression (which is seen to be quite high). All reduced sets correctly reproduce the uncertainty band for the 900 PDF Monte Carlo prior in the precision mass region and as the high mass region, while the PDF4LHC15_30 shows a certain loss in precision when reproducing uncertainties for the very low mass region.

The three techniques for delivering the PDF4LHC PDF uncertainties are attempts to match the uncertainty bands produced from the prior, and not the bands from the three PDF groups *per se*. The

degree of success is a measure of the precision of the three techniques for this purpose. It is therefore important not to confuse the precision of reproducing the prior with accuracy. The accuracy of the prior is not exactly known, especially at high and low mass, and the quoted PDF uncertainty represents only the best estimate by the PDF4LHC group.

I.2.3 Higgs boson production cross-sections

In Figure 5 we show representative inclusive Higgs boson production cross-sections in the relevant production channels at LHC with $\sqrt{s} = 13$ TeV: gluon-fusion, vector-boson fusion, associated production with a W boson, and associated production with a $t\bar{t}$ pair. These calculations have been performed with NLO matrix elements and NNLO PDFs, using MG5_aMC@NLO [54] interfaced to aMCfast [55] and applgrid [56], with the purpose of illustrating PDF uncertainties and also the relative difference between PDF sets. Indeed, since the NNLO/NLO K -factor is to a good approximation independent of PDFs, it should not affect the relative differences between the predictions of individual PDF sets. In this study, the Higgs bosons are left undecayed. No generation cuts are applied to Higgs bosons, jets or top quarks. The only selection cut that is applied is given by the fact that we assume that W and Z bosons decay leptonically, so the corresponding branching fraction is included and we require $p_T^l \geq 10$ GeV and $|\eta_l| \leq 2.5$ for the charged leptons from the weak boson decays. All uncertainties shown are pure PDF uncertainties, not including the uncertainty due to the value of α_s , which is fixed at $\alpha_s(m_Z) = 0.118$ for all cross-sections shown in the plot.

In each case, the predictions of the combined PDF4LHC15 prior and its three reduced versions, all normalized to the central value of the prior set, are shown along with the predictions from the sets which enter the combination, MMHT14, CT14 and NNPDF3.0. Predictions from the older global sets, MSTW08, CT10 and NNPDF2.3, which entered the previous prescription [28] are also shown for comparison. In particular, the better agreement for gluon-gluon fusion prediction using the new generation of PDFs (CT14, MMHT2014 and NNPDF3.0) compared to the older generation (CT10, MSTW08 and NNPDF2.3) is evident. In all cases, predictions using the reduced sets are in excellent agreement with those obtained using the prior.

In Figure 6 we show representative differential distributions for the Higgs boson production in gluon fusion, in particular the transverse momentum and rapidity distributions, at the LHC $\sqrt{s} = 13$ TeV, obtained using the three different deliveries of the combined set. The upper plots show the cross-section per bin, in pico-barns, while the lower plots show the corresponding results normalized to the central value of the PDF4LHC15 NNLO prior set. The three techniques agree well for these kinematic distributions, with a small offset for the predictions of the PDF4LHC15_mc set. Note that the transverse momentum distribution shown is a fixed-order result, and thus it is unreliable for $p_t \lesssim 30$ GeV where transverse momentum resummation effects become important.

I.2.4 Strong coupling and heavy quark masses

In order to estimate the further uncertainty due to the choice of α_s value it is useful to plot the cross-sections as a function of the value of $\alpha_s(m_Z)$. This is done in Figure 7, where the total inclusive cross-sections for Higgs boson production at $\sqrt{s} = 13$ TeV in different production channels are shown as a function of α_s for the three sets which enter the combination. In these plots we also include flavour predictions obtained using the ABM12 [40], HERAPDF2.0 [32] and JR14 [42] PDF sets, each at its preferred value of $\alpha_s(m_Z)$. In the case of ABM12, we use the $N_f = 5$ set. For HERAPDF2.0, we consider only the experimental PDF uncertainties. In the case of the JR14 set, we use the version determined in the variable-flavour-number scheme. Note that MMHT14, CT14, NNPDF3.0 and HERAPDF2.0 all use the same central value of the strong coupling, $\alpha_s(m_Z) = 0.118$; in the plot the values corresponding to these sets are slightly offset to improve readability. It is apparent from the figures which PDF sets can produce predictions that may fall substantially outside of the uncertainties of the three PDF sets that

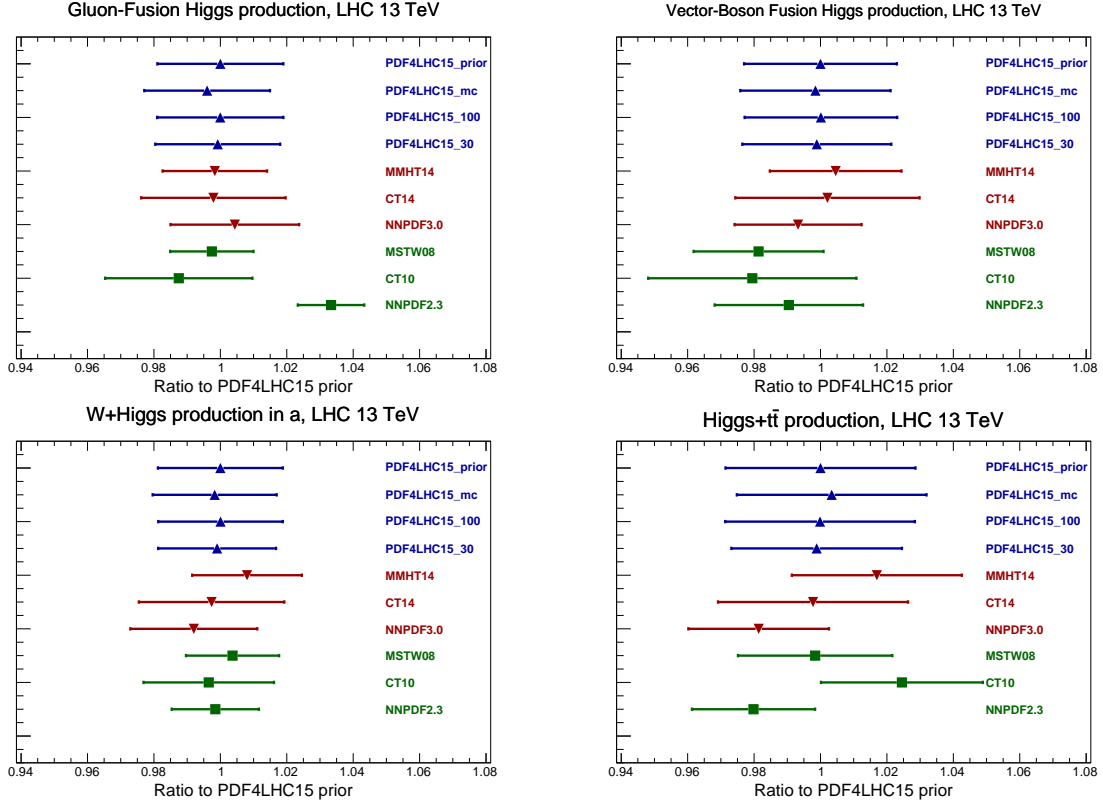


Figure 5: Inclusive Higgs boson production cross-sections at 13 TeV in the gluon-fusion, vector-boson fusion, associated production with W and associated production with a $t\bar{t}$ pair channels. In each case predictions of the three individual sets are shown along with those of the PDF4LHC15 prior and the three reduced sets, normalizing to the central value of the PDF4LHC15 prior set. Predictions obtained using the three older global sets which entered the previous PDF4LHC recommendation are also show. All cross-sections are computed at NLO with NNLO PDFs. The value of the strong coupling is fixed at $\alpha_s(m_Z) = 0.118$; the uncertainties shown are PDF uncertainties (not including the uncertainty due to $\alpha_s(m_Z)$).

enter the 2015 combination.

Unlike the case for the strong coupling $\alpha_s(M_Z)$, the different PDF groups do not use common values of the charm and bottom masses, and also use different definitions of a general mass variable number scheme (GM-VFN). These are two distinct issues, particularly since each group chooses the quark masses at fixed default values, as opposed to trying to determine them from a best fit, and the values chosen have no relation to the scheme choice.

Let us consider the issue of scheme choices first. Dependence on these has been very thoroughly studied in numerous articles [33, 57–60]. At NLO the variation in LHC cross section predictions for W and Z production due to quite extreme differences in choices of GM-VFN schemes can be of order 2 – 3%; they may be somewhat larger but still moderate especially at high scale for processes which are directly sensitive to charm, such as $Z + c$ or open charm production. However, as with other scheme choices in QCD, the ambiguity at fixed order is always an effect beyond the order of the calculation, and hence diminishes as one goes to higher orders. At NNLO scheme choices lead to changes in LHC cross section predictions of generally no more than 1%, and very often less. This can be appreciated from Figs. 11.6, 11.7 and 11.8 in [33], where differences between groups for the total HERA cross sections calculated using the same PDFs but different schemes can be at most $> 5\%$ at NLO, but never more than 1 – 2% at NNLO. Differences in $F_2^{\bar{c}c}(x, Q^2)$, an observable which is directly sensitive to charm, which is much less precisely and widely measured at HERA, can be 30% in extreme cases at NLO but are rarely

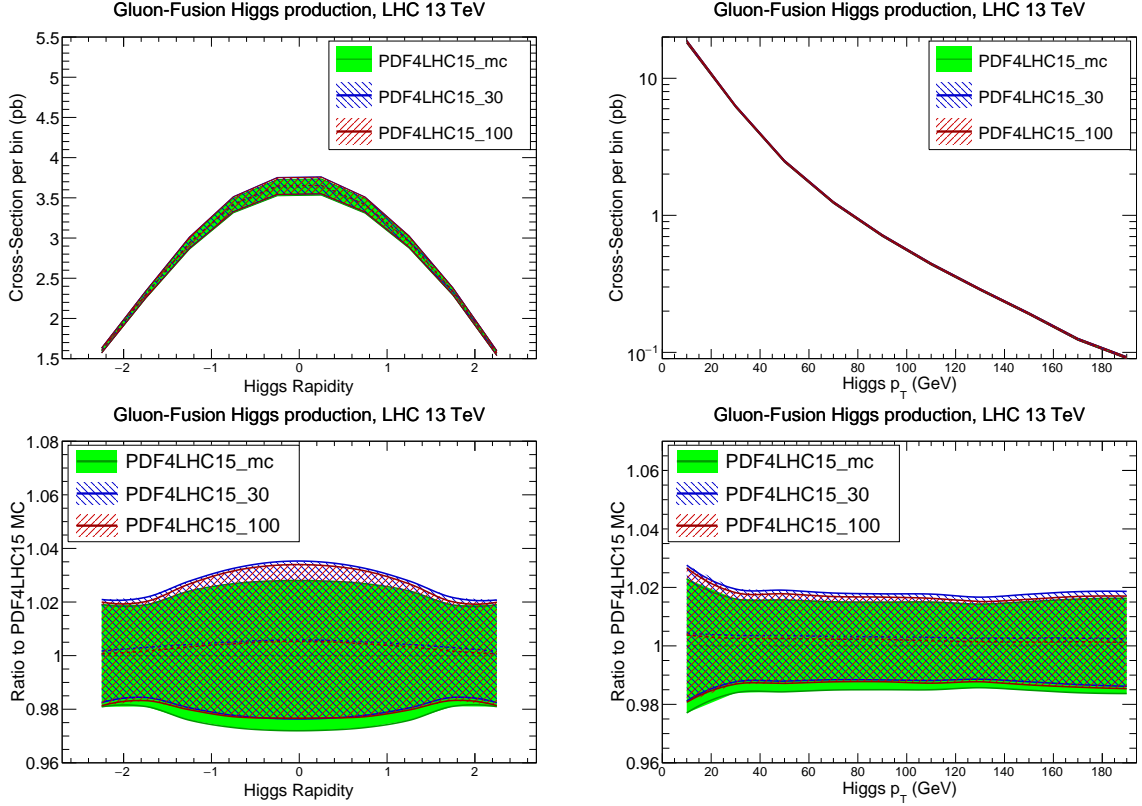


Figure 6: Differential distributions for Higgs boson production at gluon fusion at $\sqrt{s} = 13$ TeV. The Higgs boson rapidity (left) and transverse momentum (right) distributions are shown, using the three different deliveries of the combined PDF4LHC15 set. The upper plots show the absolute distributions, while in the lower plot results are normalized to the central value of the PDF4LHC15_mc set. Cross-sections have been computed at NLO with NNLO PDFs.

more than 10% at NNLO, and over most of the x, Q^2 range are much less than 5%. Hence, the variation due to the choice of GM-VFN scheme at NNLO is much less than the PDF uncertainty, and the variation between groups due to this can be taken as indicative of part on the theoretical uncertainty at NNLO. The variation due to adopting a FFN scheme would instead be quite large, and outside the PDF uncertainty.

The different PDFs used in the recommendation are all obtained using the heavy quarks defined in the pole mass scheme. However, the values chosen are different, with m_c ranging from 1.275–1.4 GeV and m_b from 4.18–4.75 GeV. The precise determinations of quark masses are performed in the $\overline{\text{MS}}$ scheme, and the conversion to the pole masses is imprecise due to a renormalon ambiguity in the conversion factor. In particular, the series for the charm quark shows essentially no convergence. Using the better behaved expression for the beauty mass, and the fact that $m_b^{\text{pole}} - m_c^{\text{pole}} = 3.4$ GeV with a very small uncertainty [27, 61], it was argued in [62] that a reasonable estimate for pole masses is $m_c^{\text{pole}} = 1.5 \pm 0.2$ GeV and $m_b^{\text{pole}} = 4.9 \pm 0.2$ GeV. Hence, the charm mass values chosen are perhaps slightly low, but not anomalous. The smallest m_b^{pole} value among the three combined sets is somewhat low, but the beauty data (including the contribution to total HERA cross sections) has extremely little constraint on PDFs in the global fit. Moreover, it has been argued that at lower orders a general mass variable flavour number scheme is not very sensitive to the scheme in which the mass is defined [63, 64]. The variation in the quark masses between groups, i.e. the deviations from the mean values, is relatively small compared to the intrinsic uncertainty for m_c , but a bit larger for m_b . As shown in [60, 64, 65], the Higgs cross section via gg fusion can vary by about 1% for m_c changes of about 0.2 GeV, while variations with m_b are much smaller than this, even for changes of 0.5 GeV. Hence, the variation in predictions

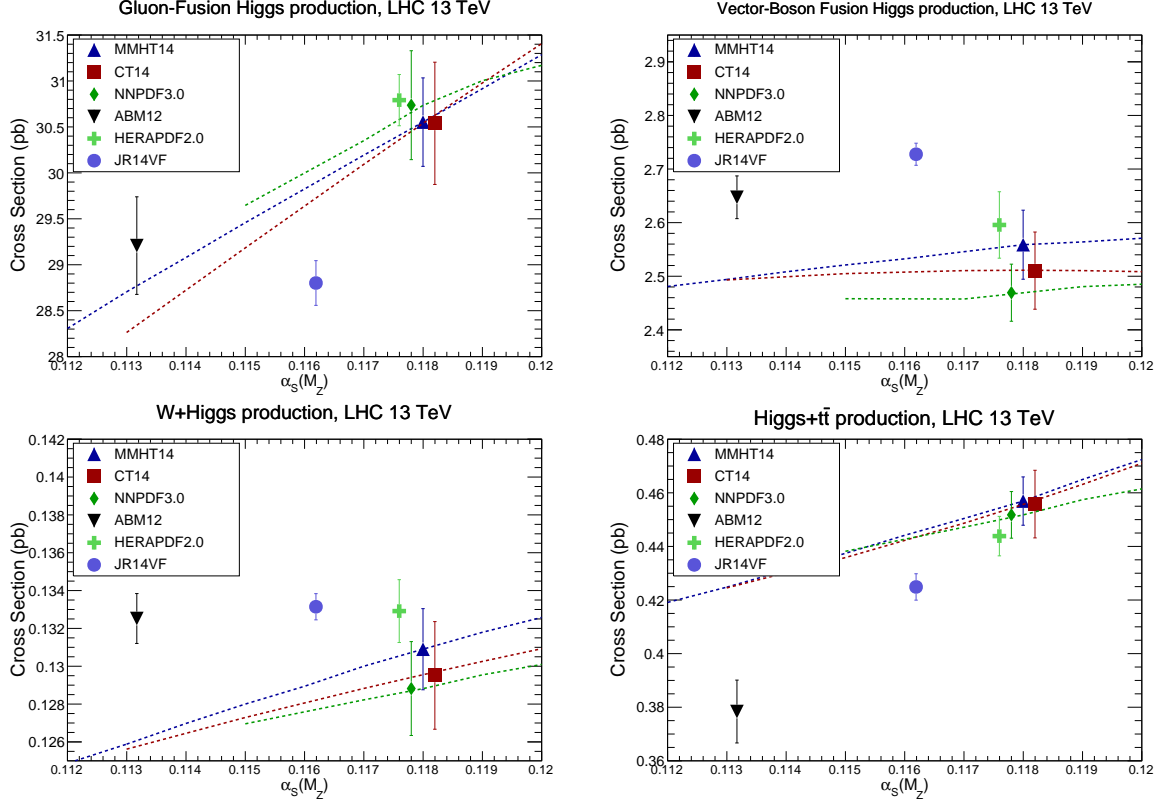


Figure 7: Dependence of the total inclusive cross-sections for Higgs boson production at $\sqrt{s} = 13$ TeV in different production channel on the value of the strong coupling $\alpha_s(m_Z)$ for the PDF sets which enter the combination: MMHT14, CT14, NNPDF3.0. Predictions obtained using ABM12, HERAPDF2.0, JR14VF NNLO sets are also shown at their preferred $\alpha_s(m_Z)$ value. The points shown for MMHT14, CT14, NNPDF3.0 and HERAPDF2.0 all refer to $\alpha_s(m_Z) = 0.118$ and are offset for clarity.

between the groups due to the different quark masses is generally much less than the PDF uncertainty, with the exception of cross sections directly dependent on the b quark distribution, where the mass effect on the distribution is more significant. The uncertainty due to quark masses should ideally be taken into account, and the current variation between groups should achieve this to some extent. However, in the future, it is probably preferable to settle on common mass values, perhaps defined in the \overline{MS} scheme as advocated in [66], and a common uncertainty, as now done for $\alpha_s(M_Z)$.

For LHC calculations that are done in the \overline{MS} scheme with up to 4 active quark flavours in the running α_s and PDFs, three combined PDF4LHC sets determined in this scheme are also provided. The respective PDF4LHC sets are constructed from 900 MC replicas of CT14, MMHT14, and NNPDF3.0 PDFs for $N_f = 4$ using the same combination techniques as for $N_f = 5$. In this case, the initial PDF parameterizations from the $N_f = 5$ fits at initial $Q_0 \sim m_c$ are evolved to higher Q including the lightest 4 flavours only. Contributions from massive bottom and top quarks should be then included in hard matrix elements. The input value $\alpha_s(M_Z, N_f = 4)$ in the $N_f = 4$ scheme is obtained from $\alpha_s(M_Z, N_f = 5) = 0.118$ by applying scheme transformation relations [67] at two or three loops in QCD, and assuming the average $m_b = 4.56$ GeV of the input PDF sets; it is thus rather smaller than the default value 0.118.

Table 1: Correlation coefficient between various Higgs boson production cross-sections and background cross-sections. In each case, the PDF4LHC15 NNLO prior set is compared to the Monte Carlo and with the two Hessian reduced sets. We also show the results from the three individual sets, CT14, MMHT14 and NNPDF3.0.

PDF Set	correlation coefficient					
	$t\bar{t}, Ht\bar{t}$	$t\bar{t}, hW$	$t\bar{t}, hZ$	$ggh, ht\bar{t}$	ggh, hW	ggh, hZ
PDF4LHC15_nnlo_prior	0.87	-0.23	-0.34	-0.13	-0.01	-0.17
PDF4LHC15_nnlo_mc	0.87	-0.27	-0.35	-0.10	0.07	-0.01
PDF4LHC15_nnlo_100	0.87	-0.24	-0.34	-0.13	-0.02	-0.17
PDF4LHC15_nnlo_30	0.87	-0.27	-0.43	-0.13	-0.04	-0.23
CT14	0.09	-0.32	-0.44	-0.26	-0.03	-0.18
MMHT14	0.90	-0.22	-0.52	0.08	-0.18	-0.33
NNPDF3.0	0.90	-0.17	-0.21	0.18	0.52	0.49

PDF Set	correlation coefficient					
	Z, W	$Z, t\bar{t}$	Z, ggh	$Z, ht\bar{t}$	Z, hW	Z, hZ
PDF4LHC15_nnlo_prior	0.89	-0.49	0.08	-0.46	0.56	0.74
PDF4LHC15_nnlo_mc	0.90	-0.44	0.18	-0.42	0.62	0.80
PDF4LHC15_nnlo_100	0.91	-0.48	0.09	-0.46	0.59	0.74
PDF4LHC15_nnlo_30	0.88	-0.63	0.04	-0.61	0.56	0.72
CT14	0.92	-0.69	0.12	-0.69	0.69	0.77
MMHT14	0.76	-0.70	0.12	-0.83	0.15	0.43
NNPDF3.0	0.96	-0.13	0.62	-0.30	0.84	0.85

PDF Set	correlation coefficient					
	$W, t\bar{t}$	W, ggh	$W, ht\bar{t}$	W, hW	W, hZ	$t\bar{t}, ggh$
PDF4LHC15_nnlo_prior	-0.40	0.20	-0.40	0.76	0.77	0.30
PDF4LHC15_nnlo_mc	-0.44	0.26	-0.42	0.81	0.82	0.32
PDF4LHC15_nnlo_100	-0.40	0.20	-0.40	0.76	0.77	0.30
PDF4LHC15_nnlo_30	-0.47	0.19	-0.47	0.77	0.76	0.31
CT14	-0.56	0.22	-0.56	0.80	0.77	0.09
MMHT14	-0.47	0.24	-0.53	0.62	0.63	0.46
NNPDF3.0	-0.08	0.64	-0.26	0.88	0.86	0.51

I.2.5 PDF correlations

Also of importance for Higgs boson predictions and analyses are the PDF correlations, both among Higgs boson production processes and between Higgs boson processes and potential background processes: tables of correlations obtained using various PDF sets were given in the previous Yellow Report [9]. These tables can now be updated using the more recent combined set. In Table 1 we collect the correlation coefficients between different Higgs boson production channels, as well as between representative Higgs boson signal and background processes. We show the results for the PDF4LHC15 NNLO prior and for the three reduced combined PDF sets, and we also include the results for the three individual PDF sets. The cross-sections have been computed at NLO with NNLO PDFs, using the same settings as in previous plots. All of the techniques do reasonably well reproducing the correlations of the prior, with the PDF4LHC15_100 PDFs reproducing the prior to within a per cent.

It should be emphasized that the values of the correlation themselves, however, can be viewed as only having a single digit (or less) accuracy in the sense that the PDF correlations for Higgs processes and backgrounds for the 3 global PDF sets can differ by the order of 0.2 (or more). For example, the spread in correlation coefficients for gluon-gluon fusion production and associated (Zh) production is 0.67. Note that the differences in the correlation coefficients between NNPDF3.0, CT14 and MMHT14 are large in many cases, though there is also good agreement in other cases.

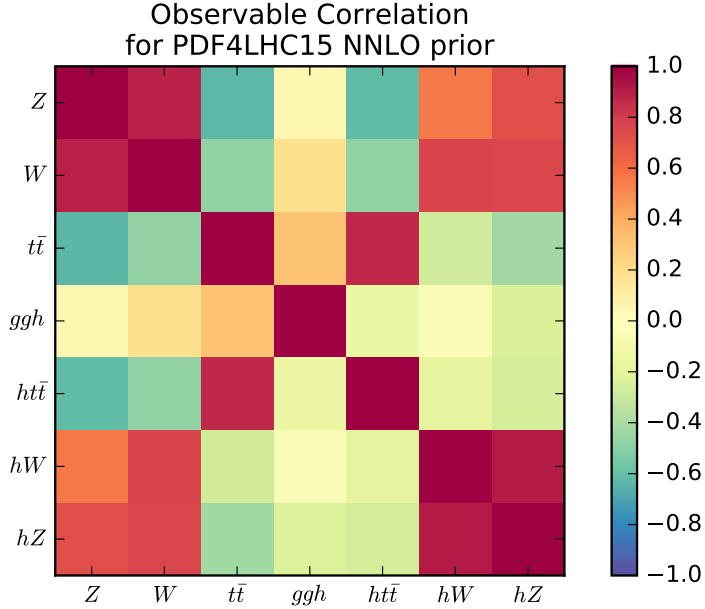


Figure 8: The value of the correlation coefficient between representative Higgs boson signal and background processes at the LHC 13 TeV, using the PDF4LHC15NNLO prior. The colour of each entry of the correlation matrix indicates the absolute size of the correlation coefficient. The processes shown in this figure are ggh , $ht\bar{t}$, hW and hZ (for signal) and Z , W and $t\bar{t}$ (for backgrounds).

In Figure 8 we show the absolute value of the correlation coefficient between representative Higgs boson signal and background processes at the LHC 13 TeV, using the PDF4LHC15NNLO prior. The colour of each entry of the correlation matrix indicates the absolute size of the correlation coefficient, with a granularity of 0.2. The processes shown in this figure are ggh , $ht\bar{t}$, hW and hZ (for signal) and Z , W and $t\bar{t}$ (for backgrounds). Very similar results are obtained if any of the three reduced sets is used.

I.2.6 Acceptance calculations

An important application of the PDF4LHC15 combined sets is the calculation of PDF uncertainties in acceptances. These are defined as the ratio of cross-sections with fiducial selection cuts to the corresponding inclusive cross-section, $\mathcal{A} = (\sigma|_{\text{fid}})/(\sigma|_{\text{incl}})$. To illustrate this usage, we have computed the acceptances, with the corresponding PDF uncertainties, for two Higgs boson production processes with experimentally realistic selection cuts, namely:

- Higgs boson production in the gluon fusion process, decaying into diphotons, $gg \rightarrow h \rightarrow \gamma\gamma$,
- Higgs boson production in association with a W boson, with the latter decaying leptonically, $pp \rightarrow hW^\pm \rightarrow hl^\pm \nu_l$.

As in the rest of this chapter, the calculations have been performed for the LHC 13 TeV with MG5_aMC@NLO interfaced to aMCfast, using NNLO PDFs with NLO matrix elements.

In the calculation of the fiducial cross-sections, we use similar acceptance requirements as those in the corresponding ATLAS and CMS analyses. For both processes, jets are reconstructed with the anti- k_T algorithm with $R = 0.4$, and they satisfy $p_T \geq 30$ GeV and $|\eta| \leq 4.4$. The additional selection cuts in the case of the $gg \rightarrow h \rightarrow \gamma\gamma$ are the following: for photons we require $p_T \geq 25$ GeV and $\eta \leq 2.4$, and the invariant mass of the diphotons should satisfy $|m_{\gamma\gamma} - 125\text{ GeV}| \leq 15\text{ GeV}$. In the case of Higgs associated production, $pp \rightarrow hW^\pm \rightarrow hl^\pm \nu_l$, the selection cuts on the charged leptons are $|\eta_l| \leq 2.5$ and $p_T^l \geq 20$ GeV.

Using these kinematical cuts, we have generated `applgrids` for both fiducial and inclusive cross-sections, and computed the resulting acceptance corrections and the corresponding PDF uncertainties. In Table 2 we collect the value of the acceptances \mathcal{A} in each case, together with the corresponding PDF uncertainties computed with the PDF4LHC15 prior and with the three reduced sets. For completeness, we also show the results for the acceptances computed with the individual PDF sets. We observe excellent agreement between the acceptances computed with the prior and with the three reduced sets, both for the central value and for the PDF uncertainties.

Table 2: The acceptance corrections \mathcal{A} for Higgs boson production at the LHC 13 TeV in two different channels with realistic selection cuts, and the corresponding PDF uncertainties. We compare the results of the PDF4LHC15 NNLO prior with the three reduced sets. For completeness, we also show the results for the acceptances computed with the individual PDF sets. See text for more details of the specific selection cuts in each case.

	$\mathcal{A}(gg \rightarrow h \rightarrow \gamma\gamma)$	$\mathcal{A}(pp \rightarrow hW \rightarrow h\nu_l)$
PDF4LHC15 prior	0.728 +- 0.006 (0.9%)	0.7536 +- 0.0014 (0.18%)
PDF4LHC15_mc	0.727 +- 0.006 (0.9%)	0.7538 +- 0.0015 (0.20%)
PDF4LHC15_100	0.728 +- 0.006 (0.9%)	0.7536 +- 0.0013 (0.17%)
PDF4LHC15_30	0.728 +- 0.006 (0.9%)	0.7536 +- 0.0012 (0.15%)
MMHT14	0.728 +- 0.004 (0.6%)	0.7532 +- 0.0012 (0.15%)
CT14	0.725 +- 0.007 (1.0%)	0.7543 +- 0.0014 (0.18%)
NNPDF3.0	0.730 +- 0.005 (0.7%)	0.7534 +- 0.0011 (0.14%)

I.2.7 Summary

To summarize, in Table 3 we collect the available PDF4LHC15 NNLO $N_f = 5$ combined sets. The corresponding sets are also available at NLO, as well as $N_f = 4$ versions. All the combined PDF4LHC14 sets are available through LHAPDF6 [43], which also includes built-in routines for the calculation of the PDF and PDF+ α_s uncertainties for all relevant cases.

Recommendations for the usage of each of these techniques are given in the PDF4LHC 2015 document [35], along with explicit formulae for the calculation of PDF and PDF+ $\alpha_s(m_Z)$ uncertainties for each of the techniques. The recommendations can be simply summed up. If asymmetric uncertainties are important, for example at high mass, and Hessian errors are not essential, then PDF4LHC15_mc should be used. There are two options for Hessian uncertainties. The PDF4LHC15_30 set provides a good estimate of the uncertainty of the prior with fewer members, sufficient in many cases, such as for the determination of nuisance parameters or acceptance calculations. To reproduce the uncertainty of the prior exactly, then the PDF4LHC_100 sets should be used.

Table 3: Summary of the combined NNLO PDF4LHC15 sets with $N_f^{\max} = 5$ that are available from LHAPDF6. The corresponding NLO sets are also available. Members 0 and 1 of PDF4LHC15_nnlo_asvar coincide with members 101 and 102 (31 and 32) of PDF4LHC15_nnlo_mc_pdfsas and PDF4LHC15_nnlo_100_pdfsas (PDF4LHC15_nnlo_30_pdfsas). Recall that in LHAPDF6 there is always a zeroth member, so that the total number of PDF members in a given set is always $N_{\text{mem}} + 1$. See text for more details.

LHAPDF6 grid	Pert order	ErrorType	N_{mem}	$\alpha_s(m_Z^2)$
PDF4LHC15_nnlo_mc	NNLO	replicas	100	0.118
PDF4LHC15_nnlo_100	NNLO	symmhessian	100	0.118
PDF4LHC15_nnlo_30	NNLO	symmhessian	30	0.118
PDF4LHC15_nnlo_mc_pdfsas	NNLO	replicas+as	102	mem 0:100 → 0.118 mem 101 → 0.1165 mem 102 → 0.1195
PDF4LHC15_nnlo_100_pdfsas	NNLO	symmhessian+as	102	mem 0:100 → 0.118 mem 101 → 0.1165 mem 102 → 0.1195
PDF4LHC15_nnlo_30_pdfsas	NNLO	symmhessian+as	32	mem 0:30 → 0.118 mem 31 → 0.1165 mem 32 → 0.1195
PDF4LHC15_nnlo_asvar	NNLO	-	1	mem 0 → 0.1165 mem 1 → 0.1195